

The imprint of dust from the North American Southwest on the California Channel Islands and Pacific Ocean sediments

Jardine, G.E.^a, Crocker A.J.^a, Bailey, I.^b, Cooper, M.J.^a, Milton, J.A.^a, and Wilson, P.A.^a

^a University of Southampton, Waterfront Campus, National Oceanography Centre, Southampton SO14 3ZH

^b Camborne School of Mines and Environment and Sustainability Institute, University of Exeter, Penryn Campus, Cornwall, UK

Corresponding Authors: A.J. Crocker. Email address: anya.crocker@noc.soton.ac.uk, P.A. Wilson Email address: paw1@noc.soton.ac.uk

Keywords: Present, Quaternary, Paleoclimatology, North America, Radiogenic isotopes

Abstract

Climate projections for the North American Southwest (NASW) predict an increasing frequency and duration of droughts over the 21st century in response to human-induced warming, with potentially severe economic and social consequences. The geological record provides a way to contextualise this prediction because of the past occurrence of abrupt hemispheric warming events and sustained intervals of atmospheric carbon dioxide loading equivalent to those projected for AD 2100 (between ~500 and 900 ppmv). Yet, terrestrial climate archives are typically too short and incomplete to provide a full record of these events. In principle, drill cores from deep sea sediments in the eastern Pacific Ocean can be used to

22 overcome this problem because they contain long records of continental dust and distal riverine-
23 supplied sediments from North America. Yet our limited understanding of the provenance and
24 transport pathways of these sediments impedes use of these marine archives for this purpose.
25 Here we present radiogenic isotope data (Sr, Nd and Pb) from known NASW dust-producing hot
26 spots – playa lakes in the Mojave Desert, Quaternary silts mantling the California Channel
27 Islands and the terrigenous fraction from marine sediments of the eastern Pacific Ocean,
28 supported by new maps of bedrock isotopic composition in the NASW. We use these and
29 published data sets to infer the origin of playa lake silts in the Mojave Desert and the source of
30 windblown sediments to the California Channel Islands and nearby ocean basins. Our results
31 rule out a significant contribution from the distal tails of either the Pacific Asian dust plume or the
32 North African dust plume to the Quaternary Channel Island silt mantles, corroborating the
33 suggestion that they are aeolian in origin and sourced from the NASW on the Santa Ana winds.
34 We identify the Outer California Borderland basins as an attractive proposition for studying past
35 dust flux and palaeoaridity in the North American South West.

36 **1 Introduction**

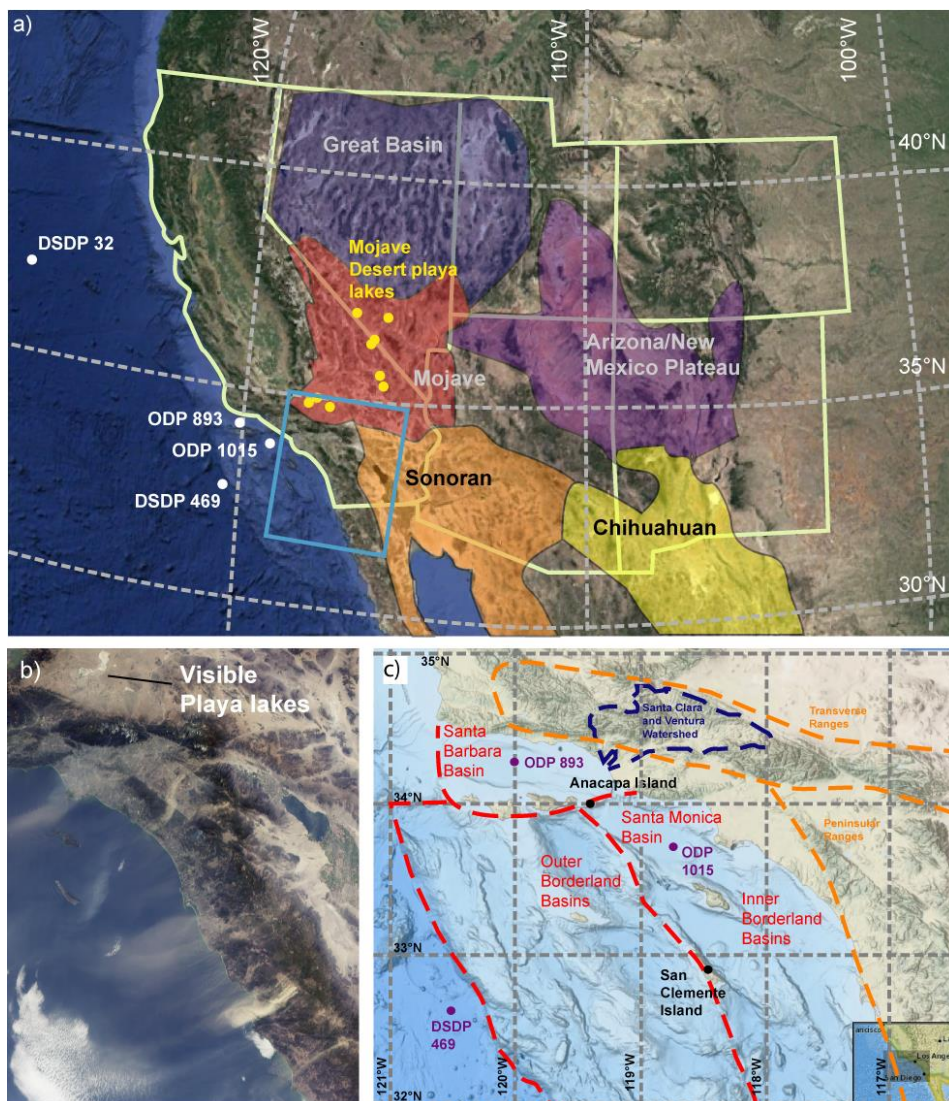
37 Climate projections to the year 2100 predict an increased frequency and duration of
38 droughts in response to human-induced warming in mid-latitude arid to semi-arid regions (Ault
39 et al., 2016; Balling and Goodrich, 2010; Cayan et al., 2010; Cook et al., 2015; Seager et al.,
40 2007). In the North American Southwest (NASW; typically taken to include the states of
41 California, Nevada, Utah, Colorado, New Mexico and Arizona, Figure 1a), these changes are
42 already evident (Ault et al., 2016; Balling and Goodrich, 2010; Cook et al., 2015; Seager et al.,
43 2007). The 2012-2016 Californian drought cost the agriculture industry an estimated \$603
44 million and the loss of over 1,500 jobs in 2016 alone (Medellín--Azuaara et al., 2016). There is a
45 pressing need, therefore, to assess the robustness of model predictions for hydroclimate in this

46 region (Cook et al., 2015; MacDonald et al., 2008).

47 Past climate records help to ground-truth future climate projections and geological data
48 provide a way to extend beyond the modern observational record by reaching deeper into the
49 past to cover a greater range of past climate conditions. Dendrochronological reconstructions
50 document numerous multi-decadal 'mega' droughts during the past 2,000 years (Cook et al.,
51 2014; Cook et al., 2007; Salzer and Kipfmüller, 2005). Although long lasting and severe
52 (decadal in length, covering at least 50% of the North American west), these megadroughts
53 occurred when atmospheric carbon dioxide levels were substantially lower than today (~280
54 ppmv during the medieval warm period, compared with ~415 ppmv, January 2021 (Ahn et al.,
55 2012; Keeling et al., 2001)) and only about one third as high as the levels predicted for 2100
56 under a 'business as usual' emissions scenario (>900 ppm under RCP 8.5 (Meinshausen et al.,
57 2011)). It is instructive, therefore, to reach deeper into the geological past, to study intervals that
58 incorporate the range of estimates for 21st century greenhouse gas levels such as the mid-
59 Piacenzian Warm Period (3.3-3 Ma) (e.g. de la Vega et al., 2020) and Miocene (e.g. Super et
60 al., 2018).

61 Lake sediments provide valuable archives of terrestrial hydroclimate in the NASW, including
62 records of variability in aeolian dust and plant leaf waxes (Feakins et al., 2014; Routson et al.,
63 2016; Tchakerian and Lancaster, 2002), but in dryland and arid-prone regions, lakes are short-
64 lived and age control can be challenging. To study pre-Quaternary palaeoclimate states, we turn
65 to marine sediment core archives, which have the potential to provide continuous, long, well-
66 dated records of terrestrial hydroclimate in deeper time (e.g. Rea, 1994; Tiedemann et al.,
67 1994). Mineral dust deposition in sediment cores can be used as a proxy for aridity in the
68 terrestrial source region because of the strong (but not necessarily simple) relationship between
69 precipitation and natural dust emissions (Hoell et al., 2014; Just et al., 2012; Larrasoana et al.,
70 2003; Nizou et al., 2011; Pettke et al., 2000; Pye, 1987b; Seo et al., 2015; Seo et al., 2014).

71 Yet, marine sediment cores may also receive terrestrial sediments sourced from rivers or ocean
 72 currents. Terrigenous flux to the marine realm cannot, therefore, always simply be interpreted
 73 as an indicator of aridity, even when those terrigenous sediments are sourced from regions that
 74 are dry today. To decipher better the climate record imprinted on sediment cores we need to
 75 distinguish between different terrigenous sources and different modes of delivery to the ocean.



76
 77 Figure 1 Study region with locations of new and previously published data reported herein: a) North
 78 American states typically included in the North American Southwest (NASW) (clockwise from left: California, Nevada,

79 Utah, Colorado, New Mexico, Arizona) with five major deserts highlighted (Google Earth imagery). Locations of
80 DSDP Sites 469 and 32, ODP Sites 893 and 1015 and the sampled Mojave Desert playa lakes (yellow filled circles)
81 also shown. Blue box in the lower left-hand corner denotes area shown in the next panel. b) MODIS Satellite imagery
82 showing dust plumes transported over the Californian Borderland Basins by the Santa Ana wind system on 9th
83 February 2002 (NASA, 2002). c) Map of southern California topography and offshore bathymetry showing location of
84 Inner and Outer Borderland Basins, the coastal Transverse and Peninsular mountain ranges, the locations of ODP
85 Sites 893 and 1015 and locations of Anacapa and San Clemente Islands.

86 Radiogenic isotopes, particularly lead (Pb), neodymium (Nd) and strontium (Sr) are valuable
87 tools to help distinguish between the provenance of sedimentary material accumulating in
88 marine settings over a wide range of spatial and temporal scales (e.g. Abouchami and Zabel,
89 2003; Cole et al., 2009; Hyeong et al., 2011; Nakai et al., 1993; Pettke et al., 2000; Seo et al.,
90 2014; Xie and Marcantonio, 2012). One particularly influential study of core-top sediments
91 characterised pelagic clays delivered to the central and eastern Pacific Ocean as a mixture of
92 three primary detrital components derived from continental source areas in Asia, Central and
93 South America and North America (Stancin et al., 2006). The fidelity of these interpretations is
94 weakened, however, by limited information on NASW sources.

95 Here we present (i) new radiogenic isotope data (Pb, Nd and Sr isotopic compositions) for
96 dust source regions in the NASW, silt mantles from the Channel Islands offshore southern
97 California and the detrital silicate fraction of young marine sediment samples from Ocean
98 Drilling Program (ODP) Sites 1015 and 893 (Figure 1a,c) and (ii) new maps of bedrock isotopic
99 composition in the NASW. We use these new data, together with published data, to improve
100 understanding of the geochemical fingerprints of terrigenous sediments transported to the
101 Pacific Ocean from the North American continent.

102 **2 Materials and Methods**

103 **2.1 Sample selection and description**

104 To investigate the export of terrigenous sediments from North America to the Pacific Ocean
105 from source to sink, we studied three main types of samples: silt mantles from two California
106 Channel Islands (Anacapa and San Clemente) proposed to derive from airborne dust from the
107 North American mainland (Muhs et al., 2007; Muhs et al., 2008), surface sediments from playa
108 lakes located in the Mojave Desert and marine sediments from two ODP Sites (1015 and 893)
109 on the California margin (Figure 1a,c). ODP Site 1015 is located in the Santa Monica Basin
110 (33°42.925'N, 118°49.185'W; Figure 1c) at 901 meters below sea level (mbsl); ODP Site 893 is
111 located in the Santa Barbara Basin (34°17.25'N, 120°02.19'W; Figure 1c) at 576.5 mbsl. The
112 Mojave Desert and island samples were obtained from the United States Geological Survey
113 (USGS), Colorado (courtesy of D. Muhs).

114 The Channel Island silt mantles are described by Muhs et al. (2007, 2008) as massive, silt-
115 rich horizons that resemble loess, or aeolian silt, ranging from 2-30cm thick, which contrast
116 sharply with the lower subsoil. Precise dating of the silt mantles on San Clemente is difficult but
117 they drape the youngest marine terrace which gives a maximum age of ~80 ka, although they
118 could possibly be younger than 3 ka, based upon a single radiocarbon data point (Muhs et al.,
119 2007). Mineralogical, geochemical and grain size profile measurements (Muhs et al., 2007;
120 Muhs et al., 2008) suggest that the dominant source of the island silt mantles is from the North
121 American continent (not from the island bedrock), implying a windblown origin, but the influence
122 of an Asian dust source (Muhs et al., 2007) and perhaps the Sahara cannot be ruled out. Muhs
123 et al. (2007) and Muhs et al. (2008) also report that the geochemical fingerprint of the fine
124 fraction (< 2 μm ; clay) in these silt mantles differs slightly from that of the coarser (2-53 μm ; silt
125 sized) fraction of the samples, hinting that the silts and clays within the silt mantles may have

126 different provenances. The identity of the North American source is equivocal – both the Mojave
127 Desert and the coastal Transverse and Peninsular mountains of Southern California have been
128 considered as potential source regions for this wind-blown material (Muhs et al., 2007; Muhs et
129 al., 2008).

130 To better characterise sources of aeolian supply to the Californian borderland from the
131 interior of the North American continent we targeted silts from the playa lakes of the Mojave
132 Desert. Playa lake and river valley sediments are known to be active sources of silt-sized
133 material for deflation and aeolian transport in dry conditions (Pye, 1987b) and offshore dust
134 transport on the Santa Ana winds that blow from the inland deserts through the mountain
135 passes of Southern California in response to high pressure systems over the Great Basin can
136 be observed in satellite imagery (Muhs et al. 2007, Figure 1b).

137 In addition to wind-borne transport of lithogenic material, the Santa Barbara and Santa
138 Monica basins also receive fluvial sediment eroded and transported by the Santa Clara and
139 Ventura River systems from the Transverse Ranges (Figure 1c), with the Santa Clara River
140 system supplying more than three times the amount of riverine material to the Santa Barbara
141 and inner borderland basins as the next largest source (Inman and Jenkins, 1999). We sampled
142 sediments of Holocene and deglacial age from ODP Sites 1015 and 893 (locations Figure 1c)
143 to fingerprint these fluvial inputs. “Riverine” samples were selected to characterise the isotopic
144 composition of fluvially derived sediments delivered to the offshore borderland basins from the
145 Californian coastal river valleys during the Late Quaternary. These consist of macroscopically
146 obvious turbidites ultimately originating from fluvial sources at Site 1015 and conspicuous cm-
147 scale ‘grey-layers’ inferred to represent fine-grained flood deposits at Site 893 (Behl, 1995;
148 Marsaglia et al., 1995). “Hemipelagic” samples were also selected at ODP Site 1015, targeting
149 intervals of background sedimentation in between the event horizons.

150 **2.2 Isotopic analyses**

151 The Channel Island silt mantle sediments were sieved to remove the >63 μm fraction,
152 following Muhs et al. (2007, 2008). A subset of these samples was also sieved over a fine mesh
153 to isolate the <10 μm fraction to allow comparison with long-range transported Asian material.
154 Prior to full chemical digestion, carbonates, organic material, biogenic silica and Fe-Mn oxides
155 were removed from the fine fraction of the sieved Channel Island samples and bulk Mojave
156 Desert playa lake silts and Californian borderland ODP sediment samples by a series of
157 chemical preparation steps, adapted from Bayon et al. (2002). Approximately 5 g of dry bulk
158 sediment was placed in sealable Nalgene conical flasks. A solution of ~10-25% acetic acid
159 solution was used to decarbonate the samples, and then 10% hydrogen peroxide solution at
160 60°C was used remove organic matter. Biogenic silica was removed from the Channel Island silt
161 mantles and California borderland ODP sediments using a 1.5M NaOH solution following the
162 method of Povea et al. (2015). Fe and Mn oxides were removed from the silt mantle and
163 borderland basin sediments using a 0.05 M hydroxylamine hydrochloride – 15% acetic acid –
164 0.03 M Na-EDTA solution buffered to pH4 with analytical grade NaOH in two steps: an initial
165 three hour reaction period; followed by the replacement of the reagent with fresh solution and a
166 second reaction period of 24 hours. For both these steps, the samples were left on a shaker
167 table. For the Mojave Desert playa lake samples, the Fe-Mn removal step was not deemed
168 necessary because tests showed no significant isotopic effect from an anthropogenic
169 contribution of Pb from a subset of samples processed with a Fe-Mn oxide removal step.

170 For Pb, Nd and Sr isotopic analyses, the chemically processed sediment samples were
171 freeze-dried and approximately 50 mg of freeze-dried sample was weighed into 15 ml Teflon
172 pots. The samples were treated with a final additional cleaning step of 1M ammonium acetate
173 solution following Pettke et al. (2000). Concentrated hydrofluoric acid (HF, ~27M) and
174 concentrated nitric acid (HNO_3 , ~12M) were added in a 5:1 ratio and the pots left to reflux at

175 ~130°C for 48 hours. Pb and Nd were then separated from the digested mother solution by ion
 176 exchange column procedures and ion selective resin for Sr. Where necessary, a modified
 177 column sequence with an additional ion exchange column was used to enhance the separation
 178 of Ba from the Sr fraction. Average digestion blanks for Pb, Nd and Sr were 320 pg, 160 pg and
 179 7 ng respectively. One digestion blank (affecting five samples) contained an anomalous
 180 concentration of Pb and was excluded from this calculation but review of the data from those
 181 five samples indicate no obvious offset with the remainder of the dataset, (see Supplementary
 182 Figure 1), so they are included herein. Average column blanks for Pb, Nd and Sr were 168 pg, 2
 183 pg and 13.5 pg respectively. The Nd-isotope ($^{143}\text{Nd}/^{144}\text{Nd}$) and Pb-isotope ratios ($^{206}\text{Pb}/^{204}\text{Pb}$,
 184 $^{207}\text{Pb}/^{204}\text{Pb}$ and $^{208}\text{Pb}/^{204}\text{Pb}$) of the samples were measured at the University of Southampton
 185 using a multi-collector inductively coupled plasma mass spectrometer (MC-ICP-MS, Thermo
 186 Scientific Neptune). Pb isotopic compositions were analysed using the double spike method of
 187 Taylor et al. (2015). The average values of NIST 981 were $16.9394 \pm < 0.0025$, $15.4955 \pm <$
 188 0.0026 and $36.7093 \pm < 0.0078$ for $^{206}\text{Pb}/^{204}\text{Pb}$, $^{207}\text{Pb}/^{204}\text{Pb}$ and $^{208}\text{Pb}/^{204}\text{Pb}$ respectively. Nd
 189 isotopic compositions were adjusted to a $^{146}\text{Nd}/^{144}\text{Nd}$ value of 0.7219 (Vance and Thirlwall,
 190 2002). Mass-bias corrected ratios were normalized to the given $^{143}\text{Nd}/^{144}\text{Nd}$ value (0.512115) of
 191 the standard JNdi-1 (Tanaka et al., 2000). The average value of JNdi-1 run as unknowns were
 192 $0.512114 \pm < 0.000006$. $^{143}\text{Nd}/^{144}\text{Nd}$ ratios are reported in epsilon notation:

$$\varepsilon_{Nd} = \left(\frac{^{143}\text{Nd}/^{144}\text{Nd}_{\text{sample}}}{^{143}\text{Nd}/^{144}\text{Nd}_{\text{CHUR}}} - 1 \right) * 10^4 \quad (1)$$

193 where $^{143}\text{Nd}/^{144}\text{Nd}_{\text{CHUR}}$ is the Chondritic Uniform Reservoir value of 0.512638 (Jacobsen and
 194 Wasserburg, 1980).

195 The $^{87}\text{Sr}/^{86}\text{Sr}$ isotopic composition of the samples was measured at the University of
 196 Southampton using a thermal ionization mass spectrometer (Thermo-Fisher TRITON Plus) with

197 an ^{88}Sr beam of 2V. Fractionation was corrected using an exponential correction normalised to
198 $^{86}\text{Sr}/^{88}\text{Sr} = 0.1194$. NIST 987 was run as a reference standard, with a long-term mean value of
199 0.710243 ± 0.000021 (2σ) reported from repeat analyses on this instrument.

200 **2.3 Radiogenic isotope base maps**

201 To place our data and the published radiogenic isotope datasets of NASW dust sources into
202 a regional context we developed Pb, Nd and Sr isotope maps of the bedrock geology by
203 compiling published measurements from the scientific literature (full reference list is given in
204 Supplementary Information). Most of the data used to develop these maps are for whole rock
205 samples, but for some data accessed through the North American Volcanic and Intrusive Rock
206 Database (NAVDAT, navdat.org), this information was not available.

207 All data were assigned latitude and longitude coordinates using published site location
208 information in conjunction with Google Earth (format X°X'X"). The location information was then
209 converted to decimal degrees and input into MATLAB_R2017a. A subset of the latitude and
210 longitude coordinates was derived by generating a path function within Google Earth and using
211 the MATLAB script `kml_shapefile.m` (Toomey, 2010) to convert the resulting .kml file to a
212 MATLAB shape file that contained the coordinate information.

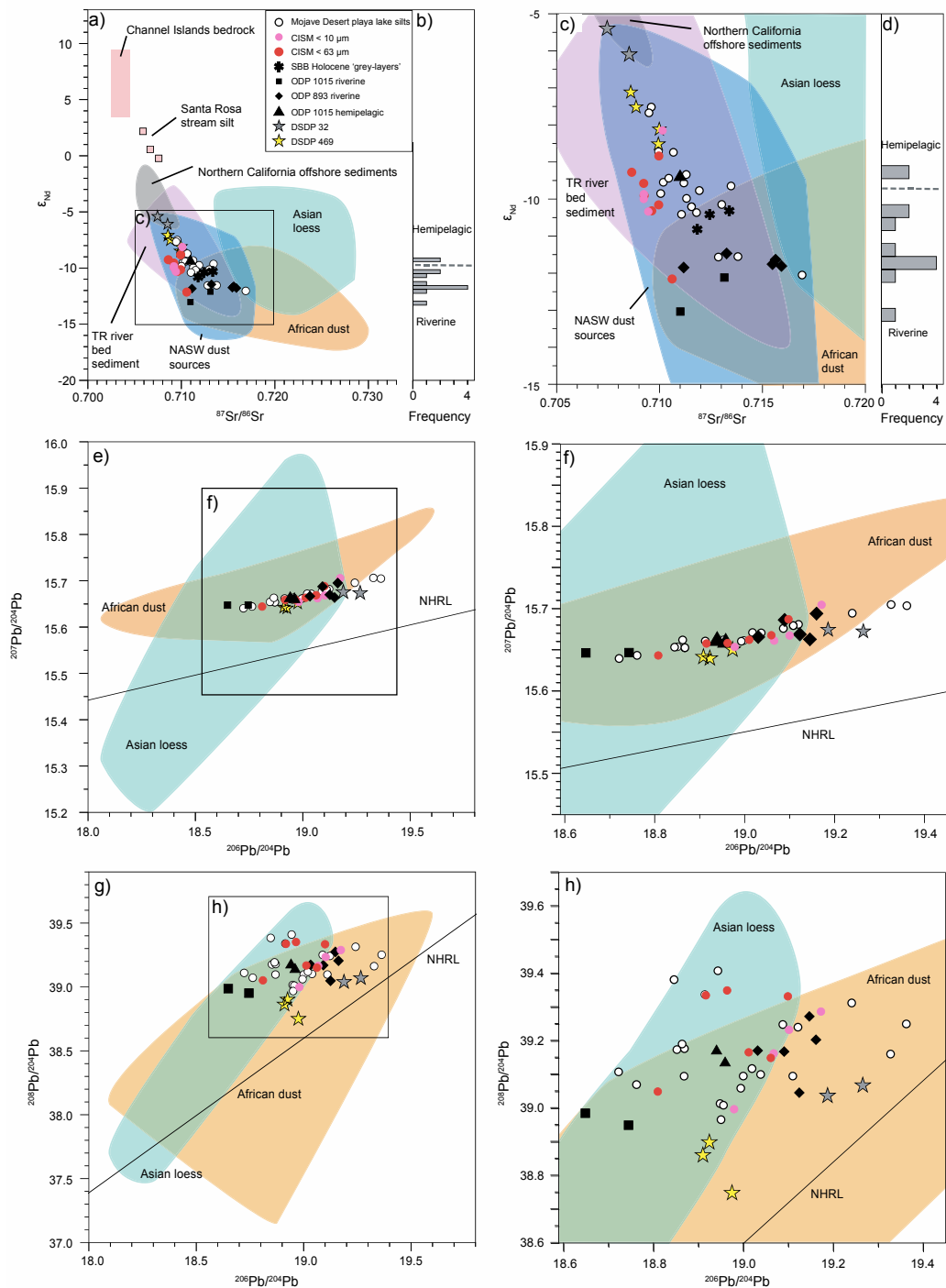
213 To generate the colour-shaded map background, the geo-referenced data were averaged
214 into $0.125^\circ \times 0.125^\circ$ latitude/longitude grid squares within the bounds of 110 to 125°W and 30 to
215 40°N. This irregularly spaced data set of grid-square-averaged isotope data points was used to
216 generate a regularly spaced 3D gridded data set, with the x and y coordinates given by the
217 latitude and longitude, and the z coordinate the associated isotopic value using the function
218 `griddata.m`. This function generated an isotopic 'data' value for the empty spaces in the original
219 data distribution using a natural interpolation function. Some samples of granitoid rocks have

220 much more radiogenic Sr values than typical rocks in the NASW, resulting in a skewed
221 distribution of $^{87}\text{Sr}/^{86}\text{Sr}$ bedrock data. As such, the grid-averaged dataset was filtered to exclude
222 $^{87}\text{Sr}/^{86}\text{Sr}$ values > 0.7350 to distinguish regional trends free of extreme local effects. $^{206}\text{Pb}/^{204}\text{Pb}$
223 isotope values > 21 were also excluded for similar reasons. Original, unfiltered maps are shown
224 in Supplementary Figure 2. The interpolation function does not allow for an extrapolation outside
225 the area bounded by data points, resulting in some regions in the map that lack a colour-coded
226 background. The gridded data set was converted to a coloured map display using the “griddata”
227 and “meshgrid” functions and projected using an equidistant conic projection system. Vector
228 files of the North American coastline, rivers, and lakes, and geotiff files of North American
229 topography were imported from the public domain database Natural Earth
230 (naturalearthdata.com).

231 **3 Results and Discussion**

232 **3.1 Isotope composition of Mojave Desert dust hotspots**

233 The Mojave Desert is an important dust-producing region that is under-characterized
234 geochemically (Urban et al., 2018). Our new Nd, Sr and Pb data for Mojave Desert playa lake
235 silts (Figure 2) improve upon existing datasets, particularly by providing a Pb isotopic
236 characterisation. The Mojave Desert playa lake silt samples that we analysed display a modest
237 range in Pb isotope compositions of 18.7217 to 19.3617 for $^{206}\text{Pb}/^{204}\text{Pb}$; internal errors are $\leq \pm$
238 0.0023. ϵ_{Nd} values range from -7.50 to -12.03 (internal errors are $\leq \pm 0.13$ epsilon units) with the
239 bulk of the distribution falling between -8.70 and -10.4 and relatively non-radiogenic $^{87}\text{Sr}/^{86}\text{Sr}$
240 ratios, ranging from 0.709447 to 0.716889; internal errors are $\leq \pm 0.000104$.



242 Figure 2 Radiogenic isotope characterisation of sources and sinks of windblown material from the NASW
 243 and nearshore eastern Pacific Ocean in: (a-d) Nd-Sr space, (e-f) $^{206}\text{Pb}/^{204}\text{Pb}$ vs $^{207}\text{Pb}/^{204}\text{Pb}$ space and (g-h)
 244 $^{206}\text{Pb}/^{204}\text{Pb}$ vs $^{208}\text{Pb}/^{204}\text{Pb}$ spaces. Panel c) shows a close-up of the Nd-Sr region outlined in a) and panels b) and d)

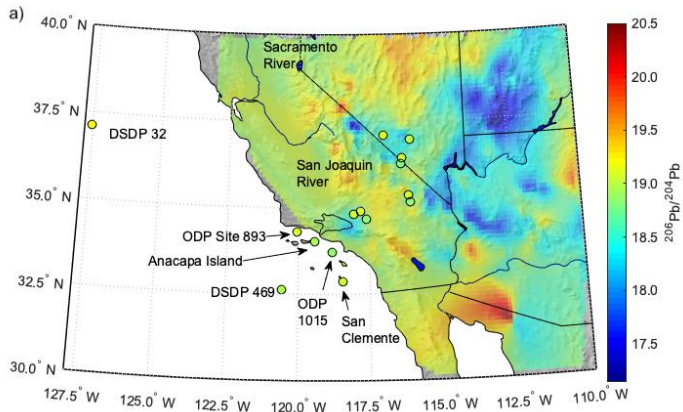
245 display histograms of the distribution of the ϵ_{Nd} isotope data from ODP Sites 893 and 1015, distinguishing between
246 'riverine' and hemipelagic samples. Panel f) shows a close-up of the $^{206}\text{Pb}/^{204}\text{Pb}$ vs $^{207}\text{Pb}/^{204}\text{Pb}$ region outlined in e).
247 Panel h) shows a close-up of the $^{206}\text{Pb}/^{204}\text{Pb}$ vs $^{208}\text{Pb}/^{204}\text{Pb}$ region outlined in g). Data for the NASW and Transverse
248 Ranges (TR) river sediment (our data, Aarons et al., 2017; Napier et al., 2020) are compared to data from Chinese
249 loess deposits, as representative of Asian dust sources (Chen et al., 2007; Jones et al., 2000; Kanayama et al., 2005;
250 Sun and Zhu, 2010; Wu et al., 2011; Zeng et al., 2015; Zhao et al., 2015, in green) and trans-Atlantic African dust
251 (Bozlaker et al., 2018; Kumar et al., 2014; Kumar et al., 2018; Meyer et al., 2011; Pourmand et al., 2014; Skonieczny
252 et al., 2013; Skonieczny et al., 2011a; van der Does et al., 2018b, in orange). Data for the Channel Island silt mantles
253 (this study), material from the California borderland basins from ODP Sites 893 and 1015 and Pacific core data (this
254 study, Napier et al., 2020; Rosenbauer et al., 2013; Stancin et al., 2006) show the isotopic composition of aeolian,
255 riverine and hemipelagic sediments sourced from North America. Nd-Sr fields of the Channel Islands bedrock
256 (Johnson and O'Neil, 1984; Weigand, 1993; Weigand and Savage, 1999) and stream bed material from Santa Rosa
257 Island (Napier et al., 2020) are also shown in panel a). Key abbreviations: CISM = Channel Island silt mantles; SBB =
258 Santa Barbara Basin. Northern Hemisphere Regression Line (NHRL) is shown on Pb isotope plots for reference
259 (Hart, 1984).

260 **3.1.1 Mojave playa lake silts versus bedrock signatures**

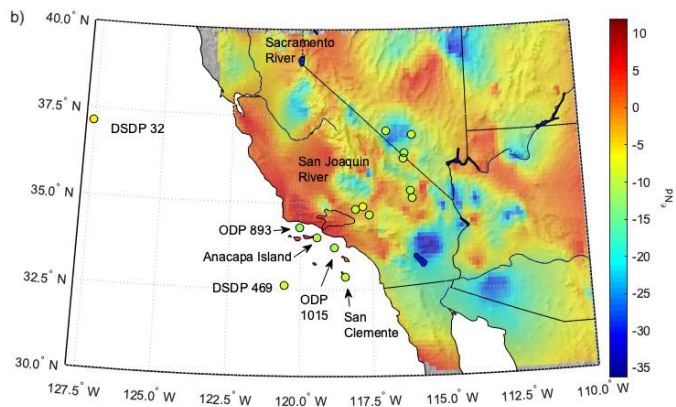
261 Radiogenic isotopes are widely used to determine the provenance of terrigenous material
262 deposited in marine sediments by comparing the isotope composition of the deposited
263 sedimentary material to the continental bedrock and surface sediments in potential source
264 regions upwind (e.g. Abouchami et al., 2013; Bailey et al., 2012; Lang et al., 2014). This
265 approach commonly necessitates averaging bedrock compositions over large areas of
266 heterogeneous geology (e.g. Lang et al., 2014; Walter et al., 2000). Our radiogenic maps allow
267 us to test the fidelity of this approach. The geomorphology of the Mojave Desert is varied, both
268 in its landforms and the geology of the country rocks (Baldrige, 2004; Jennings and Strand,
269 1981). Aeolian material from the Mojave Desert can therefore originate from a wide array of
270 country rock lithologies. In Figure 3, we compare our bedrock isotope maps to our
271 measurements of the Mojave playa lake silts to assess similarities between proximal bedrock

272 composition and aeolian material originating from the NASW. For all three isotope systems, our
273 Mojave playa lake data fall within the range of the geological bedrock of the NASW region – for
274 example, the $^{206}\text{Pb}/^{204}\text{Pb}$ isotopic composition of the geological bedrock ranges from
275 approximately 17 to 20.5, which encompasses the spread of the measured $^{206}\text{Pb}/^{204}\text{Pb}$ values of
276 the Mojave playa lake silts (~18.7 to 19.4). Some of the playas have very similar values to the
277 local bedrock (Figure 3a-c), particularly in Pb and Nd space. The Sr isotope map (Figure 3c),
278 however, clearly demonstrates that our samples from the playa lakes of the Mojave Desert are
279 typically more radiogenic in $^{87}\text{Sr}/^{86}\text{Sr}$ than their underlying bedrock. This offset is of the correct
280 sign to signal incongruent behaviour of rubidium (Rb) and Sr during weathering because that
281 process typically gives rise to more radiogenic $^{87}\text{Sr}/^{86}\text{Sr}$ values in weathered sediments than in
282 their parent bedrock (Dasch, 1969).

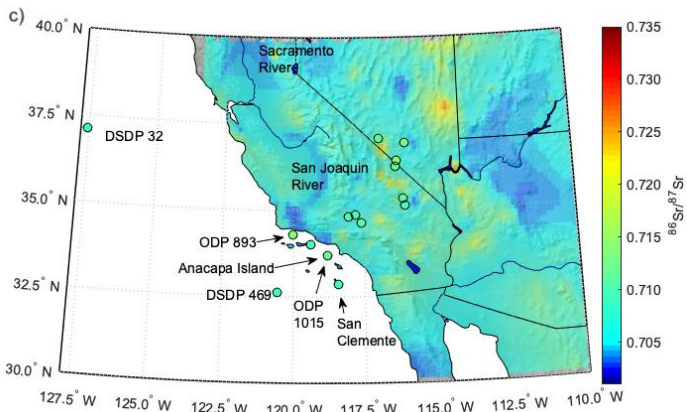
283 In summary, our Mojave Desert playa lake samples display a relatively narrow range in Pb,
284 Nd and Sr isotopic composition when compared with the bedrock. The geochemistry and
285 mineralogy of modern dust deposition in the Mojave indicates a well-mixed source of material
286 (Reynolds et al., 2006), and the isotope characteristics of our playa lake samples are likely a
287 function of this wide-scale mixing process across the desert. Next, we use these results to
288 understand better the origin of the silt mantles on the Californian Channel Islands.



289



290



291

292 Figure 3 Radiogenic isotope maps of the bedrock geology of the North American Southwest (NASW) in
 293 interpolated a) $^{206}\text{Pb}/^{204}\text{Pb}$; b) ϵ_{Nd} ; c) $^{87}\text{Sr}/^{86}\text{Sr}$ space compared to data for unconsolidated sediment samples (this
 294 study) from Mojave Playa Lake silts, Channel Island Silt Mantles, DSDP and ODP sites (coloured circles). Colour
 295 scale (right) applies to both bedrock geology and sediment samples.

296 **3.2 Origin of Channel Island silt mantles, offshore Southern California.**

297 **3.2.1 Assessing the likelihood of a significant local (island) source**

298 Satellite imagery provides strong evidence for the transport of aeolian material to the
299 Channel Islands from the NASW (Figure 1b) but the importance of aeolian supply versus a local
300 contribution from the island bedrock to the silt mantles must be carefully assessed. Contrasting
301 bedrock lithology between the NASW and Channel Islands makes this a straightforward task.
302 For the <63 μm fraction of the Channel Island silt mantles (from San Clemente and Anacapa
303 islands) ϵ_{Nd} values range from -12.14 to -8.13 with internal errors $\leq \pm 0.12$ and $^{87}\text{Sr}/^{86}\text{Sr}$ ratios
304 are unradiogenic, ranging from 0.708610 to 0.710575 with internal errors $\leq \pm 0.000083$ (Figure
305 2a). The samples are closely grouped in Pb isotope space, from 18.8088 to 19.0983 in
306 $^{206}\text{Pb}/^{204}\text{Pb}$, from 15.6439 to 15.6767 in $^{207}\text{Pb}/^{204}\text{Pb}$ and from 39.0509 to 39.3367 in $^{208}\text{Pb}/^{204}\text{Pb}$
307 space (internal errors $\leq \pm 0.0063$, 0.0058 and 0.0186, respectively; Figure 2e-h). The subset of
308 Channel Island silt mantle samples that are <10 μm have similar values in Pb isotope space to
309 the <63 μm fraction (Figure 2e-h). Their Nd isotopic values have a smaller range compared to
310 the <63 μm fraction and their average value is shifted to slightly more radiogenic (less negative)
311 ϵ_{Nd} values (-10.32 to -8.13, internal errors $\leq \pm 0.07$, Figure 2a). The measured $^{87}\text{Sr}/^{86}\text{Sr}$ values
312 (0.709194 to 0.710109, internal errors $\leq \pm 0.000072$, Figure 2a) of the <10 μm fraction fall within
313 the same range as the <63 μm fraction.

314 The isotopic values of these mantles are strikingly different to those of Channel Island
315 bedrock (Figure 2a). Whole-rock measurements of $^{87}\text{Sr}/^{86}\text{Sr}$ in San Clemente Island andesites
316 fall between 0.7037 and 0.7045 (Johnson and O'Neil, 1984). Although no bedrock Sr isotopic
317 data are available for Anacapa Island, these andesitic bedrocks are compositionally similar and
318 stratigraphically correlative to the volcanic suite on Santa Cruz Island (Weigand, 1993) which
319 has $^{87}\text{Sr}/^{86}\text{Sr}$ ratios from 0.7025 to 0.7032 (Johnson and O'Neil, 1984). Similarly, Nd isotope

320 data measured on the volcanics from the other Channel Islands (+3.4 to +9.4; Weigand and
321 Savage (1999) and references therein) serve as a good guide for the base rock composition on
322 Anacapa and San Clemente. Our data (Figure 2a) for the silt mantles contrast sharply with
323 these island bedrock compositions (and even stream bed samples from Santa Rosa Island,
324 Figure 2a, Napier et al. (2020)), providing strong support for the interpretations of Muhs et al.
325 (2007) and Muhs et al. (2008) that the island silt mantles are aeolian in origin.

326 **3.2.2 No significant input to Channel Island silts from Asia or Africa**

327 Next, we consider potential external sources of the Channel Island wind-blown silts. We
328 consider three main sources for this aeolian material: (i) the distal influence of the Pacific Asian
329 dust plume bringing material predominantly originating from East Asia (Creamean et al., 2014;
330 Uno et al., 2011; VanCuren and Cahill, 2002), (ii) aeolian material originating from Africa,
331 considered because the Sahara is the world's largest dust source (Ginoux et al., 2012; Prospero
332 et al., 2002) and African dust storms have been recorded travelling as far west as Colorado and
333 Texas (Hand et al., 2017; Perry et al., 1997), or in very rare cases, eastwards across Asia and
334 the Pacific to the western coast of North America (McKendry et al., 2007), and (iii) transport
335 from North America on the Santa Ana winds (Figure 1b; Muhs et al., 2007; Muhs et al., 2008).

336 Comparison of similar size fractions helps to minimise the widely acknowledged effects
337 exerted on $^{87}\text{Sr}/^{86}\text{Sr}$ by weathering and grain size (Dasch, 1969; Feng et al., 2009), with the fine
338 silt- and clay-sized fractions of windblown material typically carrying higher $^{87}\text{Sr}/^{86}\text{Sr}$ ratios than
339 their coarser fraction counterparts because of the preferential incorporation of K- and hence Rb-
340 rich clay and mica minerals into the finest fractions (Feng et al., 2009). Although previous
341 studies have shown that aeolian material transported over thousands of kilometres is borne
342 largely in the $<5\ \mu\text{m}$ fraction (and often even in the $<2\ \mu\text{m}$ fraction (Pye, 1987a)), it is possible
343 for larger dust particles to travel considerable distances from their source region (e.g. Betzer et

344 al., 1988; van der Does et al., 2018a) and the Channel Islands are <150 km from potential
345 mainland US dust sources. Therefore, we consider data for the total suspended sediment, loess
346 and where available, we include data measured on the <75 μm fraction. Taking this approach
347 also accounts for the break of up larger-sized dust particles during aeolian transport into finer
348 size fractions and their subsequent long-range transport.

349 To evaluate the likelihood of an Asian influence we compare our data to measurements of
350 Chinese loess deposits, which are representative of Asian-sourced dusts (Chen et al., 2007;
351 Jones et al., 2000; Kanayama et al., 2005; Sun and Zhu, 2010; Wu et al., 2011; Zeng et al.,
352 2015; Zhao et al., 2015), Figure 2. We find that the Pb isotope composition of Asian material is
353 significantly less radiogenic (Jones et al., 2000; Wu et al., 2011; Zeng et al., 2015) than that of
354 material originating from the North American continent (Figure 2e-h). The windblown island silt
355 mantles and active North American dust sources cluster along a single, well-defined trend in
356 $^{206}\text{Pb}/^{204}\text{Pb}$ vs $^{207}\text{Pb}/^{204}\text{Pb}$ space (Figure 2e-f) that is offset from the distribution of the Asian data
357 field (Figure 2e-f). There is also minimal overlap in Nd-Sr space between the Asian data and the
358 different sources of terrigenous material from the NASW (Figure 2a-c). Asian loess has a
359 broader distribution in ϵ_{Nd} space (approx. -14 to -4) and typically shows much more radiogenic
360 $^{87}\text{Sr}/^{86}\text{Sr}$ ratios than the Channel Island silts. In fact, the subset of Channel Island silt samples
361 that were sieved to <10 μm do not overlap with the Asian loess in Nd-Sr space at all (Figure 2c).
362 Thus, while Pb isotope data do not rule out the presence of Asian dust in the silt mantles when
363 considered in isolation, the Nd and Sr isotope systems together provide a powerful tool to
364 distinguish more clearly between long-range transported Asian dust and North American-
365 derived material (windblown or riverine) in Pacific sediments. Our data therefore clearly rule out
366 the possibility of a major contribution from Asia to the windblown dust deposits accumulating on
367 the California Channel Islands.

368 We next consider the likelihood of a significant deposition of trans-Atlantic African aeolian

369 material on the California Channel Islands by comparing our Channel Island silt mantle data to
370 dust trap data from North Africa, the North Atlantic and the Caribbean (Bozlaker et al., 2018;
371 Kumar et al., 2014; Kumar et al., 2018; Meyer et al., 2011; Pourmand et al., 2014; Skonieczny
372 et al., 2013; Skonieczny et al., 2011b; van der Does et al., 2018b, Figure 2). While there is
373 some overlap in Pb isotope space between our Channel Island data and the Saharan isotope
374 fields (Figure 2e-h), there is little overlap in Sr-Nd isotope space. We also note that there is a
375 poor isotopic match between the Channel Islands silt mantles and the two major North African
376 regions implicated in trans-Atlantic dust transport: the western ($^{87}\text{Sr}/^{86}\text{Sr} = 0.7279 \pm 0.0052$, $\epsilon_{\text{Nd}} =$
377 -14.79 ± 2.16) and central ($^{87}\text{Sr}/^{86}\text{Sr} = 0.7186 \pm 0.0053$, $\epsilon_{\text{Nd}} = -9.96 \pm 3.85$) preferential source
378 areas (Jewell et al., 2021). Therefore, we consider it unlikely that the Saharan dust plume
379 makes a significant contribution to sediments offshore Southern California.

380 **3.2.3 North American sources of Channel Island aeolian silt mantles**

381 Next, we evaluate possible North American sources of dust. Both the Mojave Desert and the
382 coastal mountains of Southern California are proposed as potential source regions of aeolian
383 supply to the Channel Islands (Muhs et al., 2007; Muhs et al., 2008). Both of these regions
384 contain playa lakes and river valleys, which are known sources of readily deflated silt-sized
385 material (Pye, 1987b). We compare the Sr-Nd-Pb isotope composition of the Channel Island silt
386 mantles to our Mojave playa lake silt data and other published records (Aarons et al., 2017;
387 Napier et al., 2020) in Figure 2.

388 The $<63 \mu\text{m}$ fraction of the Channel Island silt mantle samples shows a very similar trend in
389 $^{206}\text{Pb}/^{204}\text{Pb}$ vs $^{207}\text{Pb}/^{204}\text{Pb}$ space to that of the Mojave playa lake silts (Figure 2e). In $^{206}\text{Pb}/^{204}\text{Pb}$
390 vs $^{208}\text{Pb}/^{204}\text{Pb}$ space, the $<63 \mu\text{m}$ fraction of the Channel Island silt mantles are completely
391 contained within the spread of the Mojave playa lake data (Figure 2g). Thus, on the basis of our
392 Pb isotope data, the Mojave Desert is a compatible source for the aeolian material mantling the

393 Channel Islands. This conclusion is supported by the Nd isotope data because the composition
394 of the Channel Island silt mantles is very similar to the Mojave Desert samples (Figure 2a,c).
395 There is a slight discrepancy in Sr values between the Channel Island silts and the Mojave
396 Desert playa lake silts (Figure 2c) but the Channel Island data fall within the spread of dust
397 sources from the Mojave (Figure 2).

398 A geochemical characterization of the coastal mountains of southern California is provided
399 by Napier et al. (2020) who sampled streambed sediments in the coastal California Transverse
400 ranges (Figure 2a,c). There is extensive overlap in Sr-Nd space between the field described by
401 those data and our data for the Mojave playa lakes and the Channel Island silt mantles (Figure
402 2). A study of potential dust sources across a wider area of the North American West shows that
403 several other regions including the Colorado Plateau and Basin and Range province also show
404 similar radiogenic isotope fingerprints to the Mojave (Aarons et al., 2017). Therefore, we cannot
405 precisely identify the contribution to the island deposits made by each of these different source
406 regions relative to the Mojave Desert. Regardless, our data strongly support the suggestion that
407 these deposits are derived from North America (Muhs et al., 2007; Muhs et al., 2008) and the
408 pathway of the Santa Ana winds across Southern California to the offshore Pacific (Conil and
409 Hall, 2006; Hughes and Hall, 2010) suggests that active dust sources along this route, including
410 those of the Mojave, are likely to be the most important contributors to the Channel Island silt
411 mantles and surrounding ocean sediments.

412 **3.3 Distinguishing sources of terrigenous deposition offshore Southern** 413 **California**

414 The Channel Island silt mantles provide an excellent case study to characterize the
415 signature of aeolian material exported to the Eastern Pacific, but to find readily datable
416 continuous palaeoclimate archives spanning many thousands or millions of years, we must turn

417 instead to marine deposits that can contain terrigenous inputs derived via both riverine and
418 aeolian transport.

419 Previous studies investigating sediment delivery to the California borderland basins
420 concluded that fluvial input dominates the sediment budget (>80% in some parts of the inner
421 borderlands, location Figure 1c); whereas biogenic material contributes typically 20-25% (Inman
422 and Jenkins, 1999; Schwalbach and Gorsline, 1985). However, more recent work points to a
423 significant additional input of aeolian material (Muhs et al., 2007). Although the predominant
424 transport direction of dust from the NASW is eastwards on westerly winds towards the North
425 American interior and possibly the distant Atlantic Ocean (Mahowald et al., 2006), at certain
426 times during autumn and winter, 'Santa Ana' winds carry dust westwards to the Pacific Ocean
427 ((Muhs et al., 2007; Muhs et al., 2008; Reheis et al., 1995) Figure 1b). It is estimated that
428 aeolian materials contribute anywhere between 5 and 60% of the sediment deposited in the
429 California Borderlands, which varies primarily as a function of dilution by riverine material (Muhs
430 et al., 2007). Here, we explore whether radiogenic isotopes can be used to assess the relative
431 importance of aeolian and fluvial inputs to the hemipelagic sediments at ODP 893 and 1015.

432 To isolate the signature of the riverine inputs exported offshore Southern California, we
433 analysed samples from from marine drill cores at ODP Sites 893 and 1015 containing fluvial
434 deposit horizons (the ODP 893 'grey-layers' and ODP 1015 turbidites). We compare the
435 radiogenic isotope composition of hemipelagic sediments from ODP 1015 (which should contain
436 both aeolian and riverine material) to these fluvially derived horizons and to the Channel Island
437 silt mantles to understand better the relative importance of these two sources to hemipelagite
438 formation in the region. The subset of our Californian margin borderland basin samples (located
439 in the Santa Barbara and Santa Monica basins (Figure 1c)) which are dominantly fluvially
440 derived have $^{87}\text{Sr}/^{86}\text{Sr}$ values between 0.710973 and 0.715886 (internal errors $\leq \pm 0.0000073$)
441 and ϵ_{Nd} values between -13.02 and -11.45 (internal errors $\leq \pm 0.14$). The isotopic signatures of

442 the fluviually derived layers in the Santa Barbara (ODP Site 893) and Santa Monica (ODP Site
443 1015) basins are very similar, with the samples from ODP 1015 recording slightly more
444 unradiogenic ϵ_{Nd} and lower $^{206}\text{Pb}/^{204}\text{Pb}$ values (Figure 2) than ODP 893. Holocene and deglacial
445 samples from ODP Site 1015 do not show an appreciable compositional difference attributable
446 to age.

447 In Pb isotope space, the hemipelagic data are not offset from the fluviually sourced samples
448 (Figure 2e-h), but Nd-Sr measurements of the ODP core samples (Figure 2a,c) indicate a subtle
449 but quantifiable isotopic difference between horizons characterised as fluvial and 'hemipelagic
450 background' (Kennett et al., 1994; Lyle et al., 1997). The ϵ_{Nd} values of the hemipelagic material
451 (which is expected to contain both aeolian and fluvial inputs) are more radiogenic (-9.39 to -
452 9.18; internal errors $\leq \pm 0.08$) than the fluvial samples (-13.01 to -11.45) and the $^{87}\text{Sr}/^{86}\text{Sr}$
453 composition plots at the less radiogenic end of the range in the riverine samples (Figure 2b-d).

454 The distinct isotopic composition of the hemipelagic sediments from ODP Site 1015 implies
455 either a shift in the source of terrigenous material deposited in the absence of large fluvial inputs
456 to the Santa Monica Basin or a mixing of the fluvial inputs with a second, isotopically distinct
457 source of terrigenous material. Variability in the signature of the riverine inputs is supported by
458 Napier et al. (2020), who attribute more radiogenic ϵ_{Nd} and less radiogenic $^{87}\text{Sr}/^{86}\text{Sr}$ values in
459 sediment samples from the Santa Barbara Basin of Last Glacial Maximum age to an increased
460 contribution from the southern slopes of the Santa Ynez and Topatopa Mountains. Alternatively,
461 we note that hemipelagic sediment of both Holocene and deglacial age from Santa Monica
462 basin site ODP 1015 more closely resembles the Mojave Desert and Channel Island silt mantles
463 than the dominantly fluvial material sampled at the same site in Nd-Sr space, supporting a
464 greater influence of windblown dust from the NASW during times of hemipelagic deposition
465 (Figure 2a).

466 In summary, we identify differences in Sr-Nd isotopic signatures between river-derived and
467 hemipelagic sediments immediately offshore Southern California possibly attributable to
468 differences in the geochemical signatures of aeolian and riverine sediments to the Californian
469 margin. However, overlap between the isotopic signatures of terrestrial samples of source
470 regions in the Mojave, Transverse Range and greater NASW mean that it is not yet possible to
471 estimate the relative proportions of riverine and aeolian inputs to the Inner California Borderland
472 Basins using Sr-Nd-Pb isotopes (Figure 2). We therefore suggest that the Outer California
473 Borderland Basins are a more attractive proposition for studying past dust flux and palaeoaridity
474 in the North American South West.

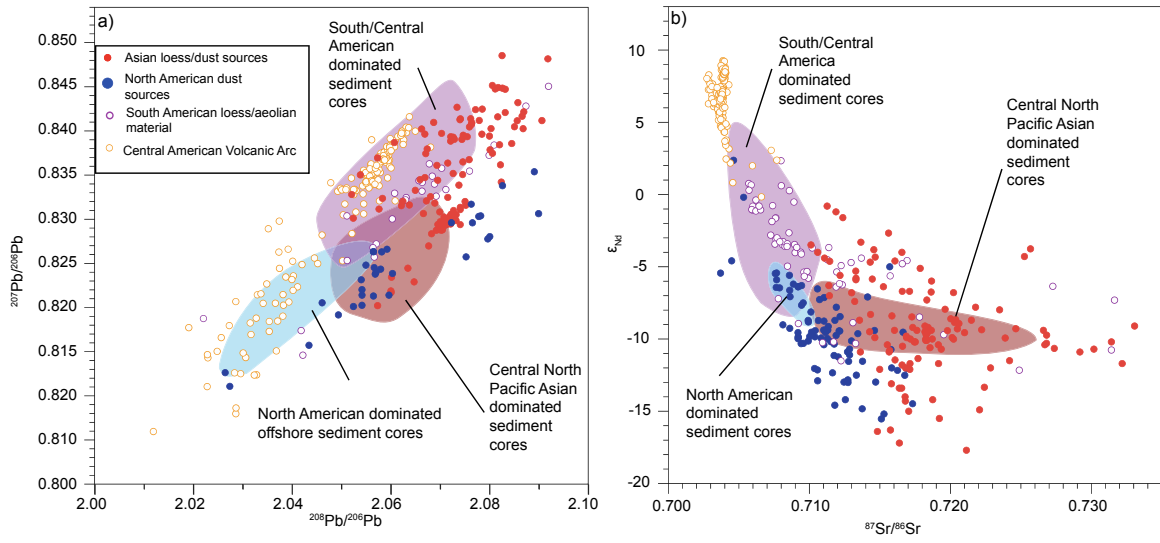
475 **3.4 Spatial variations in the geochemistry of hemipelagic deposition in the** 476 **Eastern Pacific**

477 In their pioneering study of the provenance of terrigenous input to the Pacific Ocean, Stancin
478 et al. (2006) analysed the lithogenic fraction from drill cores across the eastern Pacific to
479 determine the relative contributions from Asia, South/Central America and North America. They
480 identified two sediment core sites as containing a terrigenous fraction dominantly sourced from
481 North America: Deep Sea Drilling Project (DSDP) Sites 32 and 469. DSDP Site 469 is located at
482 32.61°N, south of ODP Sites 893 and 1015, but it is further offshore than either of these two
483 ODP Sites, situated at the base of the Patton Escarpment bounding the Southern Californian
484 Outer Borderland Basin (Figures 1 and 3). In contrast, DSDP Site 32 is located at 37.12°N, a
485 similar latitude to San Francisco Bay, approximately 820 km north of DSDP Site 469 (Figure 3).
486 Radiogenic isotope data of Plio-Pleistocene samples from these two sites were used to
487 determine the North American end member in Pb, Sr and Nd space for the entirety of the North
488 Pacific Ocean (Stancin et al., 2006). Our data provide a test of that approach.

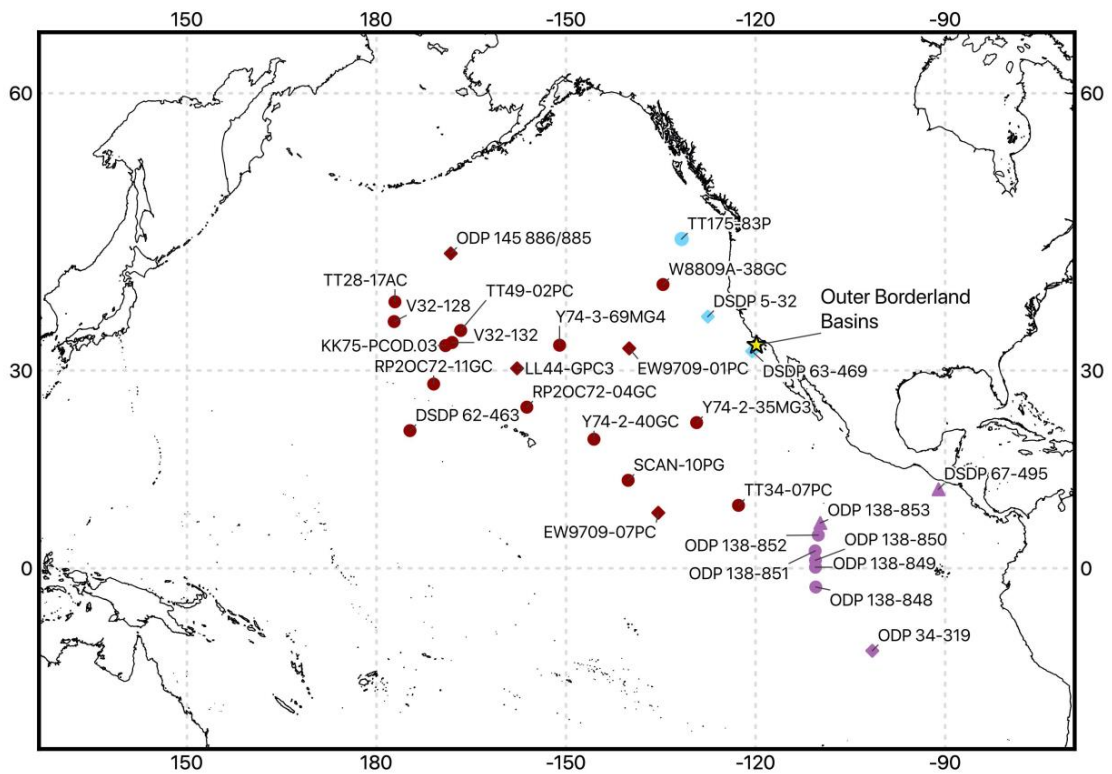
489 **3.4.1 North American terrigenous supply to the North Pacific Ocean**

490 DSDP Sites 32 and 469 are isotopically distinct from each other in Nd-Sr and Pb isotope
491 space (Figure 2). DSDP Site 32 is located (Figure 3) proximal to the Delgada Submarine Fan
492 (McManus et al., 1970), which consists of terrigenous material derived mainly from the San
493 Joaquin and Sacramento river catchments and our Pb and Sr isotope maps show good isotopic
494 agreement between the drainage basins of these two rivers (Figure 3, see also Supplementary
495 Figure 2) and DSDP Site 32. Furthermore, there is good isotopic correspondence between the
496 DSDP Site 32 data (Stancin et al., 2006) and sedimentary grab samples from the mouth and
497 near offshore of San Francisco Bay where the San Joaquin and Sacramento Rivers enter the
498 Pacific Ocean (Figure 2a, data labelled as 'Northern California offshore sediments' (Rosenbauer
499 et al., 2013)). Taken together, these lines of evidence strongly suggest that the dominant source
500 of the hemipelagic deposition at DSDP Site 32 is derived from fluvial supply from Northern
501 California.

502 DSDP Site 469 is located well to the south of DSDP Site 32, just seaward of the Southern
503 Californian Borderland basin system and the Channel Islands that lie therein (Figures 1 and 3).
504 Here, the influence of Northern Californian rivers is suggested to be minimal (Griggs and Hein,
505 1980) and our analysis substantiates this suggestion because, in contrast to DSDP 32, the
506 terrigenous fraction from DSDP 469 shows significant isotopic correspondence with Channel
507 Island silts and NASW dust sources (Figure 2, this study, Aarons et al. (2017); Stancin et al.
508 (2006)). These findings suggest that aeolian-sourced material from the NASW is a significant
509 contributor to hemipelagic deposition at DSDP 469.



510



511

512 Figure 4 Radiogenic isotope characterisation of sources of Asian, South/Central American and North
 513 American aeolian material compared to the radiogenic isotope signature recorded in eastern Pacific marine sediment
 514 cores downwind of these continents in a) $^{208}\text{Pb}/^{206}\text{Pb}$ vs $^{207}\text{Pb}/^{206}\text{Pb}$ space and b) Nd-Sr space. Panel a) displays Pb

515 isotope ratios plotted as $^{208}\text{Pb}/^{206}\text{Pb}$ vs $^{207}\text{Pb}/^{206}\text{Pb}$ to be consistent with Stancin et al. (2006). The sediment cores are
516 grouped into three fields representing the dominant source as identified by Stancin et al. (2006). We have updated
517 these three isotopic fields to include new data from both the original sites and new ones. c) Locations of the Pacific
518 marine sediment cores used to characterize the radiogenic isotope fields displayed in panels a) and b). Colours of the
519 markers correspond to the interpreted dominant source of terrigenous material at that core site. Red = Asian; blue =
520 North America; purple = South/Central America. The marker shape indicates whether the data generated from that
521 sediment core was included in the analysis of Stancin et al. (2006). Diamonds = data included by Stancin et al.
522 (2006); triangle = sediment core included in Stancin et al. (2006) from which we include additional data to calculate
523 the fields shown in panels a and b; circle = sediment core not included in Stancin et al. (2006) from which we include
524 data to calculate the fields shown in panels a and b. Data sources are given in the Supplementary Information.

525 In Figure 4 we compare the isotopic composition of the terrigenous fraction in Pacific Ocean
526 marine sediment cores with data from continental sediment sources, including our new data for
527 North America. The comparison shows much greater ranges in isotopic composition of the
528 sediment sources than the sediment sinks (the cores), highlighting the extent of signal
529 homogenisation in the marine core data caused by mixing of contributions during transport over
530 long distances.

531 Our comparisons clearly highlight the advantage of considering multiple isotope systems to
532 characterise and trace long-range aeolian transport and deposition. For example, there is
533 considerable overlap in Nd-Sr isotope space between North American sediment sources and
534 the South/Central American-dominated provenance grouping in the cores (Figure 4b) but a
535 major North American influence on the eastern equatorial North Pacific, where these cores are
536 located (see Figure 1 of Stancin et al. (2006)), can be ruled out by the fundamental mismatch in
537 Pb isotope space documented in Figure 4a.

538 **4 Conclusions**

539 We present new radiogenic isotope data to characterise sources and sinks of terrigenous

540 material originating from the North American Southwest in conjunction with new Pb, Sr and Nd
541 isotope maps of the geological bedrock of the region capturing the broad-scale features of
542 bedrock that help to trace sources and sinks of aeolian material. Our radiogenic isotope data
543 improve our ability to geochemically fingerprint terrigenous material (both aeolian and fluvial)
544 from the North American Southwest (NASW) and permit clear distinction between windblown
545 material from the NASW and long-range transported material from Asia and North Africa. We
546 rule out a significant contribution from either Asia or North Africa to the Quaternary silts mantling
547 the California Channel Islands and corroborate the suggestion that they are aeolian in origin and
548 sourced from the NASW on the Santa Ana winds.

549 We conclude that aeolian-sourced material from the NASW is a significant contributor to
550 marine sediments offshore Southern California and suggest that the Outer California Borderland
551 Basins are an attractive proposition for studying past dust export and palaeoaridity in the
552 NASW.

553 **Acknowledgements**

554 We thank D. Muhs at the USGS for samples and valuable insights during the course of this
555 research. Sediment core samples were provided by the IODP, funded by the U.S. National
556 Science Foundation and participating countries. We are also grateful to R. Taylor and A.
557 Michalik for laboratory assistance and constructive discussions and to two anonymous
558 reviewers whose comments greatly improved this manuscript. This study was supported by the
559 University of Southampton in the form of a Mayflower Scholarship to G.E.J. I.B. acknowledges
560 funding from an EU MARINEFF project (Interreg VA France-(Channel)-England Programme
561 project #162). P.A.W. and A.J.C. acknowledge Royal Society funding including a Wolfson Merit
562 Award to P.A.W.

563 **Data availability**

564 The data presented in this manuscript will be made available upon request. These data will
565 be deposited in PANGAEA upon acceptance of this manuscript for publication.

566 **References**

- 567 Aarons, S.M., Blakowski, M.A., Aciego, S.M., Stevenson, E.I., Sims, K.W.W., Scott, S.R.,
568 Aarons, C., 2017. Geochemical characterization of critical dust source regions in the American
569 West. *Geochimica Et Cosmochimica Acta* 215, 141-161.
- 570 Abouchami, W., Näthe, K., Kumar, A., Galer, S.J.G., Jochum, K.P., Williams, E., Horbe, A.M.C.,
571 Rosa, J.W.C., Balsam, W., Adams, D., Mezger, K., Andreae, M.O., 2013. Geochemical and
572 isotopic characterization of the Bodélé Depression dust source and implications for transatlantic
573 dust transport to the Amazon Basin. *Earth and Planetary Science Letters* 380, 112-123.
- 574 Abouchami, W., Zabel, M., 2003. Climate forcing of the Pb isotope record of terrigenous input
575 into the Equatorial Atlantic. *Earth and Planetary Science Letters* 213, 221-234.
- 576 Ahn, J., Brook, E.J., Mitchell, L., Rosen, J., McConnell, J.R., Taylor, K., Etheridge, D., Rubino,
577 M., 2012. Atmospheric CO₂ over the last 1000 years: A high-resolution record from the West
578 Antarctic Ice Sheet (WAIS) Divide ice core. *Global Biogeochemical Cycles* 26.
- 579 Ault, T.R., Mankin, J.S., Cook, B.I., Smerdon, J.E., 2016. Relative impacts of mitigation,
580 temperature, and precipitation on 21st-century megadrought risk in the American Southwest.
581 *Science Advances* 2.
- 582 Bailey, I., Foster, G.L., Wilson, P.A., Jovane, L., Storey, C.D., Trueman, C.N., Becker, J., 2012.
583 Flux and provenance of ice-rafted debris in the earliest Pleistocene sub-polar North Atlantic
584 Ocean comparable to the last glacial maximum. *Earth and Planetary Science Letters* 341-344,
585 222-233.
- 586 Baldrige, W.S., 2004. *Geology of the American Southwest: A Journey through Two Billion*
587 *years of Plate-Tectonic History*. Cambridge University Press, United Kingdom.
- 588 Balling, R.C., Goodrich, G.B., 2010. INCREASING DROUGHT IN THE AMERICAN
589 SOUTHWEST? A CONTINENTAL PERSPECTIVE USING A SPATIAL ANALYTICAL
590 EVALUATION OF RECENT TRENDS. *Physical Geography* 31, 293-306.
- 591 Bayon, G., German, C.R., Boella, R.M., Milton, J.A., Taylor, R.N., Nesbitt, R.W., 2002. An
592 improved method for extracting marine sediment fractions and its application to Sr and Nd
593 isotopic analysis. *Chemical Geology* 187, 179-199.
- 594 Behl, R.J., 1995. Sedimentary facies and sedimentology of the late Quaternary Santa Barbara
595 Basin, Site 893. *Proceedings of the Ocean Drilling Program; Scientific Results* 146, 295-308.
- 596 Betzer, P.R., Carder, K.L., Duce, R.A., Merrill, J.T., Tindale, N.W., Uematsu, M., Costello, D.K.,
597 Young, R.W., Feely, R.A., Breland, J.A., Bernstein, R.E., Greco, A.M., 1988. Long-range
598 transport of giant mineral aerosol particles. *Nature* 336, 568-571.
- 599 Bozlaker, A., Prospero, J.M., Price, J., Chellam, S., 2018. Linking Barbados Mineral Dust
600 Aerosols to North African Sources Using Elemental Composition and Radiogenic Sr, Nd, and Pb
601 Isotope Signatures. *Journal of Geophysical Research: Atmospheres* 123, 1384-1400.
- 602 Cayan, D.R., Das, T., Pierce, D.W., Barnett, T.P., Tyree, M., Gershunov, A., 2010. Future
603 dryness in the southwest US and the hydrology of the early 21st century drought. *Proceedings*
604 *of the National Academy of Sciences of the United States of America* 107, 21271-21276.

- 605 Chen, J., Li, G.J., Yang, J.D., Rao, W.B., Lu, H.Y., Balsam, W., Sun, Y.B., Ji, J.F., 2007. Nd and
606 Sr isotopic characteristics of Chinese deserts: Implications for the provenances of Asian dust.
607 *Geochimica Et Cosmochimica Acta* 71, 3904-3914.
- 608 Cole, J.M., Goldstein, S.L., Demenocal, P.B., Hemming, S.R., Grousset, F.E., 2009. Contrasting
609 compositions of Saharan dust in the eastern Atlantic Ocean during the last deglaciation and
610 African Humid Period. *Earth and Planetary Science Letters* 278, 257-266.
- 611 Conil, S., Hall, A., 2006. Local Regimes of Atmospheric Variability: A Case Study of Southern
612 California. *Journal of Climate* 19, 4308-4325.
- 613 Cook, B.I., Ault, T.R., Smerdon, J.E., 2015. Unprecedented 21st century drought risk in the
614 American Southwest and Central Plains. *Sci. Adv* 1, e1400082.
- 615 Cook, B.I., Smerdon, J.E., Seager, R., Cook, E.R., 2014. Pan-Continental Droughts in North
616 America over the Last Millennium. *Journal of Climate* 27, 383-397.
- 617 Cook, E.R., Seager, R., Cane, M.A., Stahle, D.W., 2007. North American drought:
618 Reconstructions, causes, and consequences. *Earth-Science Reviews* 81, 93-134.
- 619 Creamean, J.M., Spackman, J.R., Davis, S.M., White, A.B., 2014. Climatology of long-range
620 transported Asian dust along the West Coast of the United States. *Journal of Geophysical*
621 *Research: Atmospheres* 119, 2014JD021694.
- 622 Dasch, E.J., 1969. Strontium isotopes in weathering profiles, deep-sea sediments, and
623 sedimentary rocks. *Geochimica et Cosmochimica Acta* 33, 1521-1552.
- 624 de la Vega, E., Chalk, T.B., Wilson, P.A., Bysani, R.P., Foster, G.L., 2020. Atmospheric CO₂
625 during the Mid-Piacenzian Warm Period and the M2 glaciation. *Scientific Reports* 10, 11002.
- 626 Feakins, S.J., Kirby, M.E., Cheetham, M.I., Ibarra, Y., Zimmerman, S.R.H., 2014. Fluctuation in
627 leaf wax D/H ratio from a southern California lake records significant variability in isotopes in
628 precipitation during the late Holocene. *Organic Geochemistry* 66, 48-59.
- 629 Feng, J.L., Zhu, L.P., Zhen, X.L., Hu, Z.G., 2009. Grain size effect on Sr and Nd isotopic
630 compositions in eolian dust: Implications for tracing dust provenance and Nd model age.
631 *Geochemical Journal* 43, 123-131.
- 632 Ginoux, P., Prospero, J.M., Gill, T.E., Hsu, N.C., Zhao, M., 2012. Global-scale attribution of
633 anthropogenic and natural dust sources and their emission rates based on MODIS Deep Blue
634 aerosol products. *Reviews of Geophysics* 50, RG3005.
- 635 Griggs, G.B., Hein, J.R., 1980. Sources, Dispersal, and Clay Mineral Composition of Fine-
636 Grained Sediment off Central and Northern California. *The Journal of Geology* 88, 541-566.
- 637 Hand, J.L., Gill, T.E., Schichtel, B.A., 2017. Spatial and seasonal variability in fine mineral dust
638 and coarse aerosol mass at remote sites across the United States. *Journal of Geophysical*
639 *Research: Atmospheres* 122, 3080-3097.
- 640 Hart, S.R., 1984. A large-scale isotope anomaly in the Southern Hemisphere mantle. *Nature*
641 309, 753-757.
- 642 Hoell, A., Funk, C., Barlow, M., 2014. The regional forcing of Northern hemisphere drought
643 during recent warm tropical west Pacific Ocean La Nina events. *Climate Dynamics* 42, 3289-

- 644 3311.
- 645 Hughes, M., Hall, A., 2010. Local and synoptic mechanisms causing Southern California's
646 Santa Ana winds. *Climate Dynamics* 34, 847-857.
- 647 Hyeong, K., Kim, J., Pettke, T., Yoo, C.M., Hur, S.-d., 2011. Lead, Nd and Sr isotope records of
648 pelagic dust: Source indication versus the effects of dust extraction procedures and authigenic
649 mineral growth. *Chemical Geology* 286, 240-251.
- 650 Inman, D.L., Jenkins, S.A., 1999. Climate Change and the Episodicity of Sediment Flux of Small
651 California Rivers. *The Journal of Geology* 107, 251-270.
- 652 Jacobsen, S.B., Wasserburg, G.J., 1980. SM-ND ISOTOPIC EVOLUTION OF CHONDRITES.
653 *Earth and Planetary Science Letters* 50, 139-155.
- 654 Jennings, C.W., Strand, R.G., 1981. *Geologic Map of California*, 5th ed.
- 655 Jewell, A.M., Drake, N., Crocker, A.J., Bakker, N.L., Kunkelova, T., Bristow, C.S., Cooper, M.J.,
656 Milton, J.A., Breeze, P.S., Wilson, P.A., 2021. Three North African dust source areas and their
657 geochemical fingerprint. *Earth and Planetary Science Letters*, 116645.
- 658 Johnson, C.M., O'Neil, J.R., 1984. Triple junction magmatism: a geochemical study of Neogene
659 volcanic rocks in western California. *Earth and Planetary Science Letters* 71, 241-262.
- 660 Jones, C.E., Halliday, A.N., Rea, D.K., Owen, R.M., 2000. Eolian inputs of lead to the North
661 Pacific. *Geochimica et Cosmochimica Acta* 64, 1405-1416.
- 662 Just, J., Heslop, D., von Döbeneck, T., Bickert, T., Dekkers, M.J., Frederichs, T., Meyer, I.,
663 Zabel, M., 2012. Multiproxy characterization and budgeting of terrigenous end-members at the
664 NW African continental margin. *Geochemistry Geophysics Geosystems* 13.
- 665 Kanayama, S., Yabuki, S., Zeng, F., Liu, M., Shen, Z.-z., Liu, L., Yanagisawa, F., Abe, O., 2005.
666 Size-dependent geochemical characteristics of Asian dust - Sr and Nd isotope compositions as
667 tracers for source identification. *Journal of the Meteorological Society of Japan* 83, 107-120.
- 668 Keeling, C.D., Piper, S.C., Bacastow, R.B., Wahlen, M., Whorf, T.P., Heimann, M., Meijer, H.A.,
669 2001. Exchanges of atmospheric CO₂ and ¹³CO₂ with the terrestrial biosphere and oceans
670 from 1978 to 2000. *Scripps Institution of Oceanography*, San Diego.
- 671 Kennett, J.P., Baldauf, J.G., Shipboard Scientific Party, 1994. Visual core description from ODP
672 Hole 143-893B.
- 673 Kumar, A., Abouchami, W., Galer, S.J.G., Garrison, V.H., Williams, E., Andreae, M.O., 2014. A
674 radiogenic isotope tracer study of transatlantic dust transport from Africa to the Caribbean.
675 *Atmospheric Environment* 82, 130-143.
- 676 Kumar, A., Abouchami, W., Galer, S.J.G., Singh, S.P., Fomba, K.W., Prospero, J.M., Andreae,
677 M.O., 2018. Seasonal radiogenic isotopic variability of the African dust outflow to the tropical
678 Atlantic Ocean and across to the Caribbean. *Earth and Planetary Science Letters* 487, 94-105.
- 679 Lang, D.C., Bailey, I., Wilson, P.A., Beer, C.J., Bolton, C.T., Friedrich, O., Newsam, C.,
680 Spencer, M.R., Gutjahr, M., Foster, G.L., Cooper, M.J., Milton, J.A., 2014. The transition on
681 North America from the warm humid Pliocene to the glaciated Quaternary traced by eolian dust
682 deposition at a benchmark North Atlantic Ocean drill site. *Quaternary Science Reviews* 93, 125-

683 141.

684 Larrasoana, J.C., Roberts, A.P., Rohling, E.J., Winkhofer, M., Wehausen, R., 2003. Three
685 million years of monsoon variability over the northern Sahara. *Climate Dynamics* 21, 689-698.

686 Lyle, M., Koizumi, I., Richter, C., Shipboard Scientific Party, 1997. Visual core description from
687 ODP Hole 167-1015B.

688 MacDonald, G.M., Stahle, D.W., Diaz, J.V., Beer, N., Busby, S.J., Cerano-Paredes, J., Cole,
689 J.E., Cook, E.R., Endfield, G., Gutierrez-Garcia, G., Hall, B., Magan, V., Meko, D.M., Méndez-
690 Pérez, M., Sauchyn, D.J., Watson, E., Woodhouse, C.A., 2008. Climate Warming and 21st-
691 Century Drought in Southwestern North America. *Eos, Transactions American Geophysical*
692 *Union* 89, 82-82.

693 Mahowald, N.M., Muhs, D.R., Levis, S., Rasch, P.J., Yoshioka, M., Zender, C.S., Luo, C., 2006.
694 Change in atmospheric mineral aerosols in response to climate: Last glacial period,
695 preindustrial, modern, and doubled carbon dioxide climates. *Journal of Geophysical Research:*
696 *Atmospheres* 111, n/a-n/a.

697 Marsaglia, K.M., Rimkus, K.C., Behl, R.J., 1995. Provenance of sand deposited in the Santa
698 Barbara Basin at Site 893 during the last 155,000 years. *Proceedings of the Ocean Drilling*
699 *Program; Scientific Results* 146, 61-75.

700 McKendry, I.G., Strawbridge, K.B., O'Neill, N.T., Macdonald, A.M., Liu, P.S.K., Leaitch, W.R.,
701 Anlauf, K.G., Jaegle, L., Fairlie, T.D., Westphal, D.L., 2007. Trans-Pacific transport of Saharan
702 dust to western North America: A case study. *Journal of Geophysical Research: Atmospheres*
703 112.

704 McManus, D.A., Burns, R.E., von der Borch, C.C., Goll, R.M., Milow, E.D., Olsson, R.K., Vallier,
705 T., Weser, O., 1970. Site 32. Affiliation (analytic): Univ. Wash., Seattle, WA 5, 15.

706 Medellín--Azura, J., MacEwan, D., Howitt, R.E., Sumner, D.A., Lund, J.R., 2016. Economic
707 Impacts of the 2016 California Drought for Agriculture, p. 17.

708 Meinshausen, M., Smith, S.J., Calvin, K., Daniel, J.S., Kainuma, M.L.T., Lamarque, J.F.,
709 Matsumoto, K., Montzka, S.A., Raper, S.C.B., Riahi, K., Thomson, A., Velders, G.J.M., van
710 Vuuren, D.P.P., 2011. The RCP greenhouse gas concentrations and their extensions from 1765
711 to 2300. *Climatic Change* 109.

712 Meyer, I., Davies, G.R., Stuut, J.-B.W., 2011. Grain size control on Sr-Nd isotope provenance
713 studies and impact on paleoclimate reconstructions: An example from deep-sea sediments
714 offshore NW Africa. *Geochemistry, Geophysics, Geosystems* 12.

715 Muhs, D.R., Budahn, J., Reheis, M., Beann, J., Skipp, G., Fisher, E., 2007. Airborne dust
716 transport to the eastern Pacific Ocean off southern California: Evidence from San Clemente
717 Island. *Journal of Geophysical Research-Atmospheres* 112.

718 Muhs, D.R., Budahn, J.R., Johnson, D.L., Reheis, M., Beann, J., Skipp, G., Fisher, E., Jones,
719 J.A., 2008. Geochemical evidence for airborne dust additions to soils in Channel Islands
720 National Park, California. *Geological Society of America Bulletin* 120, 106-126.

721 Nakai, S., Halliday, A.N., Rea, D.K., 1993. PROVENANCE OF DUST IN THE PACIFIC-OCEAN.
722 *Earth and Planetary Science Letters* 119, 143-157.

- 723 Napier, T.J., Hendy, I.L., Fahnestock, M.F., Bryce, J.G., 2020. Provenance of detrital sediments
724 in Santa Barbara Basin, California, USA: Changes in source contributions between the Last
725 Glacial Maximum and Holocene. *GSA Bulletin* 132, 65-84.
- 726 NASA, 2002. *Dusty Skies over Southern California*
- 727 Nizou, J., Hanebuth, T.J.J., Vogt, C., 2011. Deciphering signals of late Holocene fluvial and
728 aeolian supply from a shelf sediment depocentre off Senegal (north-west Africa). *Journal of*
729 *Quaternary Science* 26, 411-421.
- 730 Perry, K.D., Cahill, T.A., Eldred, R.A., Dutcher, D.D., Gill, T.E., 1997. Long-range transport of
731 North African dust to the eastern United States. *Journal of Geophysical Research: Atmospheres*
732 102, 11225-11238.
- 733 Pettke, T., Halliday, A.N., Hall, C.M., Rea, D.K., 2000. Dust production and deposition in Asia
734 and the north Pacific Ocean over the past 12 Myr. *Earth and Planetary Science Letters* 178,
735 397-413.
- 736 Pourmand, A., Prospero, J.M., Sharifi, A., 2014. Geochemical fingerprinting of trans-Atlantic
737 African dust based on radiogenic Sr-Nd-Hf isotopes and rare earth element anomalies. *Geology*
738 42, 675-678.
- 739 Povea, P., Cacho, I., Moreno, A., Menendez, M., Mendez, F.J., 2015. A new procedure for the
740 lithic fraction characterization in marine sediments from high productivity areas: Optimization of
741 analytical and statistical procedures. *Limnology and Oceanography-Methods* 13, 127-137.
- 742 Prospero, J.M., Ginoux, P., Torres, O., Nicholson, S.E., Gill, T.E., 2002. Environmental
743 characterization of global sources of atmospheric soil dust identified with the NIMBUS 7 Total
744 Ozone Mapping Spectrometer (TOMS) absorbing aerosol product. *Reviews of Geophysics* 40,
745 1002.
- 746 Pye, K., 1987a. Chapter 3 - DUST ENTRAINMENT, TRANSPORT AND DEPOSITION, Aeolian
747 Dust and Dust Deposits. Academic Press, pp. 29-62.
- 748 Pye, K., 1987b. Chapter 4 - DUST SOURCES, SINKS AND RATES OF DEPOSITION, Aeolian
749 Dust and Dust Deposits. Academic Press, pp. 63-91.
- 750 Rea, D.K., 1994. The paleoclimatic record provided by eolian deposition in the deep sea: The
751 geologic history of wind. *Reviews of Geophysics* 32, 159-195.
- 752 Reheis, M.C., Goodmacher, J.C., Harden, J.W., McFadden, L.D., Rockwell, T.K., Shroba, R.R.,
753 Sowers, J.M., Taylor, E.M., 1995. QUATERNARY SOILS AND DUST DEPOSITION IN
754 SOUTHERN NEVADA AND CALIFORNIA. *Geological Society of America Bulletin* 107, 1003-
755 1022.
- 756 Reynolds, R.L., Reheis, M., Yount, J., Lamothe, P., 2006. Composition of aeolian dust in natural
757 traps on isolated surfaces of the central Mojave Desert—Insights to mixing, sources, and
758 nutrient inputs. *Journal of Arid Environments* 66, 42-61.
- 759 Rosenbauer, R.J., Foxgrover, A.C., Hein, J.R., Swarzenski, P.W., 2013. A Sr–Nd isotopic study
760 of sand-sized sediment provenance and transport for the San Francisco Bay coastal system.
761 *Marine Geology* 345, 143-153.
- 762 Routson, C.C., Overpeck, J.T., Woodhouse, C.A., Kenney, W.F., 2016. Three Millennia of

- 763 Southwestern North American Dustiness and Future Implications. *Plos One* 11.
- 764 Salzer, M.W., Kipfmüller, K.F., 2005. Reconstructed temperature and precipitation on a
765 millennial timescale from tree-rings in the Southern Colorado Plateau, USA. *Climatic Change*
766 70, 465-487.
- 767 Schwalbach, J.R., Gorsline, D.S., 1985. HOLOCENE SEDIMENT BUDGETS FOR THE
768 BASINS OF THE CALIFORNIA CONTINENTAL BORDERLAND. *Journal of Sedimentary*
769 *Petrology* 55, 829-842.
- 770 Seager, R., Ting, M., Held, I., Kushnir, Y., Lu, J., Vecchi, G., Huang, H.-P., Harnik, N., Leetmaa,
771 A., Lau, N.-C., Li, C., Velez, J., Naik, N., 2007. Model Projections of an Imminent Transition to a
772 More Arid Climate in Southwestern North America. *Science* 316, 1181-1184.
- 773 Seo, I., Lee, Y.I., Kim, W., Yoo, C.M., Hyeong, K., 2015. Movement of the Intertropical
774 Convergence Zone during the mid-pleistocene transition and the response of atmospheric and
775 surface ocean circulations in the central equatorial Pacific. *Geochemistry Geophysics*
776 *Geosystems* 16, 3973-3981.
- 777 Seo, I., Lee, Y.I., Yoo, C.M., Kim, H.J., Hyeong, K., 2014. Sr-Nd isotope composition and clay
778 mineral assemblages in eolian dust from the central Philippine Sea over the last 600 kyr:
779 Implications for the transport mechanism of Asian dust. *Journal of Geophysical Research:*
780 *Atmospheres* 119, 2014JD022025.
- 781 Skonieczny, C., Bory, A., Bout-Roumazielles, V., Abouchami, W., Galer, S.J.G., Crosta, X.,
782 Diallo, A., Ndiaye, T., 2013. A three-year time series of mineral dust deposits on the West
783 African margin: Sedimentological and geochemical signatures and implications for interpretation
784 of marine paleo-dust records. *Earth and Planetary Science Letters* 364, 145-156.
- 785 Skonieczny, C., Bory, A., Bout-Roumazielles, V., Abouchami, W., Galer, S.J.G., Crosta, X.,
786 Stuut, J.B., Meyer, I., Chiapello, I., Podvin, T., Chatenet, B., Diallo, A., Ndiaye, T., 2011a. The
787 7–13 March 2006 major Saharan outbreak: Multiproxy characterization of mineral dust
788 deposited on the West African margin. *Journal of Geophysical Research: Atmospheres* 116.
- 789 Skonieczny, C., Bory, A., Bout-Roumazielles, V., Abouchami, W., Galer, S.J.G., Crosta, X.,
790 Stuut, J.B., Meyer, I., Chiapello, I., Podvin, T., Chatenet, B., Diallo, A., Ndiaye, T., 2011b. The
791 7–13 March 2006 major Saharan outbreak: Multiproxy characterization of mineral dust
792 deposited on the West African margin. *Journal of Geophysical Research: Atmospheres* 116.
- 793 Stancin, A.M., Gleason, J.D., Rea, D.K., Owen, R.M., Moore, T.C., Blum, J.D., Hovan, S.A.,
794 2006. Radiogenic isotopic mapping of late Cenozoic eolian and hemipelagic sediment
795 distribution in the east-central Pacific. *Earth and Planetary Science Letters* 248, 840-850.
- 796 Sun, J.M., Zhu, X.K., 2010. Temporal variations in Pb isotopes and trace element
797 concentrations within Chinese eolian deposits during the past 8 Ma: Implications for provenance
798 change. *Earth and Planetary Science Letters* 290, 438-447.
- 799 Super, J.R., Thomas, E., Pagani, M., Huber, M., O'Brien, C., Hull, P.M., 2018. North Atlantic
800 temperature and pCO₂ coupling in the early-middle Miocene. *Geology* 46, 519-522.
- 801 Tanaka, T., Togashi, S., Kamioka, H., Amakawa, H., Kagami, H., Hamamoto, T., Yuhara, M.,
802 Orihashi, Y., Yoneda, S., Shimizu, H., Kunimaru, T., Takahashi, K., Yanagi, T., Nakano, T.,
803 Fujimaki, H., Shinjo, R., Asahara, Y., Tanimizu, M., Dragusanu, C., 2000. JNdi-1: a neodymium

804 isotopic reference in consistency with LaJolla neodymium. *Chemical Geology* 168, 279-281.

805 Taylor, R.N., Ishizuka, O., Michalik, A., Milton, J.A., Croudace, I.W., 2015. Evaluating the
806 precision of Pb isotope measurement by mass spectrometry. *Journal of Analytical Atomic*
807 *Spectrometry* 30, 198-213.

808 Tchakerian, V.P., Lancaster, N., 2002. Late quaternary arid/humid cycles in the Mojave Desert
809 and western Great Basin of North America. *Quaternary Science Reviews* 21, 799-810.

810 Tiedemann, R., Sarnthein, M., Shackleton, N.J., 1994. Astronomic timescale for the Pliocene
811 Atlantic $\delta^{18}\text{O}$ and dust flux records of Ocean Drilling Program Site 659. *Paleoceanography* 9,
812 619-638.

813 Toomey, M., 2010. KML to SHP conversion using kml_shapefile, 1.2.0.0 ed, MATLAB Central
814 File Exchange.

815 Uno, I., Eguchi, K., Yumimoto, K., Liu, Z., Hara, Y., Sugimoto, N., Shimizu, A., Takemura, T.,
816 2011. Large Asian dust layers continuously reached North America in April 2010. *Atmos. Chem.*
817 *Phys.* 11, 7333-7341.

818 Urban, F.E., Goldstein, H.L., Fulton, R., Reynolds, R.L., 2018. Unseen Dust Emission and
819 Global Dust Abundance: Documenting Dust Emission from the Mojave Desert (USA) by Daily
820 Remote Camera Imagery and Wind-Erosion Measurements. *Journal of Geophysical Research-*
821 *Atmospheres* 123, 8735-8753.

822 van der Does, M., Knippertz, P., Zschenderlein, P., Giles Harrison, R., Stuut, J.-B.W., 2018a.
823 The mysterious long-range transport of giant mineral dust particles. *Science Advances* 4.

824 van der Does, M., Pourmand, A., Sharifi, A., Stuut, J.-B.W., 2018b. North African mineral dust
825 across the tropical Atlantic Ocean: Insights from dust particle size, radiogenic Sr-Nd-Hf isotopes
826 and rare earth elements (REE). *Aeolian Research* 33, 106-116.

827 Vance, D., Thirlwall, M., 2002. An assessment of mass discrimination in MC-ICPMS using Nd
828 isotopes. *Chemical Geology* 185, 227-240.

829 VanCuren, R.A., Cahill, T.A., 2002. Asian aerosols in North America: Frequency and
830 concentration of fine dust. *Journal of Geophysical Research: Atmospheres* 107, AAC 19-11-
831 AAC 19-16.

832 Walter, H.J., Hegner, E., Diekmann, B., Kuhn, G., Rutgers van der loeff, M.M., 2000.
833 Provenance and transport of terrigenous sediment in the south Atlantic Ocean and their
834 relations to glacial and interglacial cycles: Nd and Sr isotopic evidence. *Geochimica et*
835 *Cosmochimica Acta* 64, 3813-3827.

836 Weigand, P., 1993. Geochemistry and Origin of Middle Miocene Volcanic Rocks from Santa
837 Cruz and Anacapa Islands, Southern California Borderland. Santa Barbara Museum of Natural
838 History, Santa Barbara, CA.

839 Weigand, P.W., Savage, K.L., 1999. Summary of the Miocene Igneous rocks of the Channel
840 Islands, Southern California, in: Browne, D.R.H., Chaney, H., Mitchell, eds. (Eds.), Fifth
841 Californian Islands Symposium.

842 Wu, F., Ho, S.S.H., Sun, Q.L., Ip, S.H.S., 2011. Provenance of Chinese Loess: Evidence from
843 Stable Lead Isotope. *Terr. Atmos. Ocean. Sci.* 22, 305-314.

- 844 Xie, R.F.C., Marcantonio, F., 2012. Deglacial dust provenance changes in the Eastern
845 Equatorial Pacific and implications for ITCZ movement. *Earth and Planetary Science Letters*
846 317, 386-395.
- 847 Zeng, F., Liang, M., Peng, S., Yu, D., Xiang, S., 2015. Sr-Nd-Pb Isotopic Compositions of the
848 Neogene Eolian Deposits in the Xining Basin and Implications for Their Dust Sources. *Journal*
849 *of Earth Science* 26, 669-676.
- 850 Zhao, W., Sun, Y., Balsam, W., Zeng, L., Lu, H., Otgonbayar, K., Ji, J., 2015. Clay-sized Hf-Nd-
851 Sr isotopic composition of Mongolian dust as a fingerprint for regional to hemispherical
852 transport. *Geophysical Research Letters* 42, 5661-5669.
- 853